



1 **Identifying robust bias adjustment methods for extreme precipitation in**
2 **a pseudo-reality setting**

3

4 Torben Schmith¹, Peter Thejll¹, Peter Berg², Fredrik Boberg¹, Ole Bøssing Christensen¹, Bo Christiansen¹,
5 Jens Hesselbjerg Christensen^{1,3,4}, Christian Steger⁵, Marianne Sloth Madsen¹

6

7 ¹ Danish Meteorological Institute, Lyngbyvej 100, 2100 Copenhagen Ø, Denmark

8 ² Swedish Meteorological and Hydrological Institute, Hydrology Research Unit, Norrköping, Sweden

9 ³ Physics of Ice, Climate and Earth, Niels Bohr Institute, University of Copenhagen, 2100 Copenhagen Ø,
10 Denmark

11 ⁴ NORCE Norwegian Research Centre, Bjerknes Centre for Climate Research, 5007 Bergen, Norway

12 ⁵ Deutscher Wetterdienst, Frankfurter Straße 135, 63067 Offenbach, Germany

13

14 Correspondence: Torben Schmith (ts@dmi.dk)

15

16

17 **Abstract**

18 Severe precipitation events occur rarely and are often localized in space and of short duration; but they are
19 important for societal managing of infrastructure. Therefore, there is a demand for estimating future
20 changes in the statistics of these rare events. These are usually projected using Regional Climate Model
21 (RCM) scenario simulations combined with extreme value analysis to obtain selected return levels of
22 precipitation intensity. However, due to imperfections in the formulation of the physical parameterizations
23 in the RCMs, the simulated present-day climate usually has biases relative to observations. Therefore, the
24 RCM results are often bias-adjusted to match observations. This does, however, not guarantee that bias-
25 adjusted projected results will match future reality better, since the bias may change in a changed climate.
26 In the present work we evaluate different bias adjustment techniques in a changing climate. This is done in
27 an inter-model cross-validation setup, in which each model simulation in turn plays the role of pseudo-
28 reality, against which the remaining model simulations are bias adjusted and validated. The study uses
29 hourly data from present-day and RCP8.5 late 21st century from 19 model simulations from the EURO-
30 CORDEX ensemble at 0.11° resolution, from which fields of selected return levels are calculated for hourly
31 and daily time scale. The bias adjustment techniques applied to the return levels are based on extreme
32 value analysis and include analytical quantile-matching together with the simpler climate factor approach.
33 Generally, return levels can be improved by bias adjustment, compared to obtaining them from raw
34 scenarios. The performance of the different methods depends of the time scale considered. On hourly time
35 scale, the climate factor approach performs better than the quantile-matching approaches. On daily time
36 scale, the superior approach is to simply deduce future return levels from observations and the second best
37 choice is using the quantile-mapping approaches. These results are found in all European sub-regions
38 considered.

39



40 **1 Introduction**

41 Severe precipitation events occur either as stratiform day-long precipitation of moderate intensity or as
42 localized cloudbursts lasting a few hours only. Such extreme events may cause flooding with the risk of loss
43 of life and damage to infrastructure. It is expected that future changes in the radiative forcing from
44 greenhouse gases and other forcing agents will influence the large scale atmospheric conditions, such as air
45 mass humidity, vertical stability, and typical low pressure tracks. Therefore also the statistics of the
46 occurrence of severe precipitation events will most likely change.

47

48 Global climate models (GCMs) is the main tool for estimating future climate conditions. A GCM is a global
49 representation of the atmosphere, the ocean and the land surface, and the interaction between these
50 components. The GCM is then forced with observed greenhouse gas concentrations, atmospheric
51 compositions, land use, etc. to represent the past and present climate, and with stipulated scenarios of
52 future concentrations of radiative agents to represent the future climate.

53

54 Present state-of-the art GCMs from the Coupled Model Intercomparison Project Phase 5 (CMIP5, Taylor et
55 al. 2012) and the recent Coupled Model Intercomparison Project Phase 6 (CMIP6, Eyring et al. 2016)
56 typically have a grid spacing of around 100 km or even more. This resolution is too coarse to describe the
57 effect of regional and local features, such as mountains, coast lines and lakes and to adequately describe
58 convective precipitation systems (Eggert et al. 2015). To model the processes on smaller spatial scales,
59 dynamical downscaling is applied. Here, the atmospheric and surface fields from a GCM simulation are used
60 as boundary conditions for a regional climate model (RCM) over a smaller region with a much finer grid
61 spacing, at present typically around 10 km or even less.

62

63 The ability of present-day RCMs to reproduce observed extreme precipitation statistics on daily and sub-
64 daily time scales is essential and has been of concern. Earlier studies analysing this topic have mostly
65 focused on a particular country, probably due to the lack of sub-daily observational data covering larger
66 regions, such as e.g. Europe. Thus, Hanel and Buishand (2010), Kendon et al. (2014), Olsson et al. (2015)
67 and Sunyer et al. (2017) studied daily and hourly extreme precipitation in different European countries and
68 reached similar conclusions: first that the bias of extreme statistics decreases with smaller grid spacing of
69 the model, and second that extreme statistics for 24 h duration are satisfactorily simulated with a grid
70 spacing of 10 km, while 1 h extreme statistics exhibits biases even at this resolution. Recently, Berg et al.
71 (2019) have evaluated high resolution RCMs from the EURO-CORDEX ensemble (Jacob et al. 2014) and
72 came up with similar conclusions for several countries across Europe: RCMs underestimate hourly extremes
73 and give an erroneous spatial distribution.

74

75 Extreme convective precipitation of short duration is thus one of the more challenging phenomena to
76 describe physically in RCMs. The reason is that convective events take place on a spatial scale comparable
77 to the RCM grid spacing of presently around 10 km. Therefore, the convective plumes cannot be directly
78 modelled. Instead, the effects of convection are parametrised, i.e. modelled as processes on larger spatial
79 scales. Thus, the inability to reproduce these short duration extremes can be explained by the imperfect
80 parametrization of sub-grid scale convection, which generally leads to too early onset of convective rainfall
81 in the diurnal cycle and subsequent dampening of the build-up of convective available potential energy
82 (CAPE, Trenberth et al. 2003).



83

84 Thus, even RCMs with their small grid spacing may exhibit systematic biases for variables related to
85 convective precipitation. If there is a substantial bias, we should consider adjusting for this bias. Bias
86 adjustment techniques are thoroughly discussed, including requirements and limitations, in Maraun (2016)
87 and Maraun et al. (2017). There are two main bias adjustment approaches. In the *delta-change* approach, a
88 transformation is established from the present to the future climate in the model run. This transformation
89 is then applied to the observations to get the projected future climate. In the *bias correction* approach, a
90 transformation is established from present model climate data to the observed climate and this
91 transformation is then applied to the future model climate to obtain the projected future climate.

92

93 Both adjustment approaches come in several flavours. In the simplest one, the transformation consists of
94 an adjustment of the mean, in the case of precipitation by multiplying the mean by a factor. In the more
95 elaborate flavour, the transformation is defined by quantile-matching, preserving also the higher moments.
96 Quantile-matching adjustment can use either empirical quantiles or analytical distribution functions. The
97 ability of quantile-matching to reduce bias has been demonstrated for daily precipitation in present-day
98 climate using observations, which are split into training and verification parts (Piani et al. 2010; Themeßl et
99 al. 2011).

100

101 Bias adjustment techniques originate in the field of weather and ocean forecast modelling, where output is
102 adjusted for model deficiencies and local features. Applying similar bias adjustment techniques to climate
103 model simulations, however, has a complication not present in weather and ocean forecast applications:
104 Climate models are set up and tuned to present-day conditions and verified against observations, but then
105 applied to future changed conditions without any possibility to directly verify the model's performance
106 under these conditions. Consequently, showing that bias adjustment works for present-day climate is a
107 necessary but not sufficient condition for the adjustment to work in the changed climate.

108

109 In practical applications of bias adjustment methods to climate simulations, it is generally assumed that the
110 bias of the model is unchanged from the present-day climate to the future climate (stationarity). Only a few
111 examples has pointed out directly how to validate this cornerstone assumption (see however Buser et al.
112 (2010) and Boberg and Christensen (2012)) and therefore it is not obvious that applying bias adjustment
113 improve projections of future climate characteristics. We also note that the bias adjustment methods
114 themselves may influence the climate change signal of the model, depending on the bias and the correction
115 method used (Haerter et al. 2011; Berg et al. 2012; Themeßl et al. 2012).

116

117 One approach to partly overcome the above challenge and evaluate the total performance of bias
118 adjustment methods is *inter-model cross-validation*, as pursued by Maraun (2012), Räisänen and Rätty
119 (2013) and Rätty et al. (2014). The rationale is that the members in a multi-model ensemble of simulations
120 represent different descriptions of physics of the climate system, with each of them being not too far from
121 the real climate system. In the cross-validation exercise, one member of the ensemble in turn plays the role
122 of *pseudo-reality*, against which the remaining bias-adjusted models are evaluated. Thus, the trick is that
123 we know both present and future pseudo-reality.

124



125 Inter-model cross-validation has been applied on daily precipitation to evaluate different adjustment
126 methods (Räty et al. 2014). Here we apply a similar methodology European-wide to extreme precipitation
127 on hourly and daily time scale. This has been possible with the advent of the EURO-CORDEX, a large
128 ensemble of high-resolution RCM simulations with precipitation in hourly time-resolution. Being more
129 specific, we will apply the standard extreme value analysis to the ensemble of model data for present-day
130 and end-21st-century conditions to estimate return levels for daily and hourly duration. Then we will apply
131 inter-model cross validation on these return levels in order to address the following questions:

- 132 1. Do bias-adjusted return levels perform better, according to the inter-model cross-validating, than
133 using un-corrected model data from scenario simulations?
- 134 2. Is there any difference in performance between different adjustment methods?
- 135 3. Are there systematic differences in point 1 and 2, depending on the daily and hourly duration?
- 136 4. Are there regional differences across Europe in the performance of the different techniques?

137 Giving qualified answers to these questions can serve as important guidelines for analysis procedures for
138 obtaining future extreme precipitation characteristics.

139
140 The rest of the paper contains a description of the EURO-CORDEX data (Section 2) and a description of
141 methods used (Section 3). Then follow the results (Section 4), a discussion of these (Section 5) and finally a
142 summary (Section **Fejl! Henvisningskilde ikke fundet.**).

143

144 **2 The EURO-CORDEX data**

145 The model simulations used here have been performed within the framework of EURO-CORDEX (Jacob et
146 al. (2014) ; <http://euro-cordex.net>), which is an international effort aimed at providing RCM climate
147 simulations for a specific European region (see Figure 1) in two standard resolutions with a grid spacing of
148 0.44° (EUR-44, ~50 km) and 0.11° (EUR-11, ~12.5 km), respectively. All GCM simulations driving the RCMs
149 follow the CMIP5 protocol (Taylor et al. 2012) and are forced with historical forcing for the period 1951-
150 2005 followed by the RCP8.5 scenario for the period 2006-2100 (until 2099 only for HadGEM-ES).

151

152 We analyse precipitation data in hourly time-resolution from 19 different GCM-RCM combinations from the
153 EUR-11 simulations shown in Table 1 and we analyse two 25 year long time slices from each of these
154 simulations: a present-day time slice (years 1981-2005) and an end-21st-century time slice (years 2075-
155 2099).

156

157 All GCM-RCM combinations we use are represented by one realization only, and therefore the data
158 material used represents 19 different possible realisations of climate model physics, though acknowledging
159 that some GCMs/RCMs might originate from the same or similar ancestor and therefore may not be fully
160 independent. The EURO-CORDEX ensemble includes a few simulations, which do not use the standard EUR-
161 11 grid. These were not included in the analysis, since they should have been re-gridded to the EUR-11 grid
162 which would dampen extreme events, thus introducing an unnecessary error source.

163

164

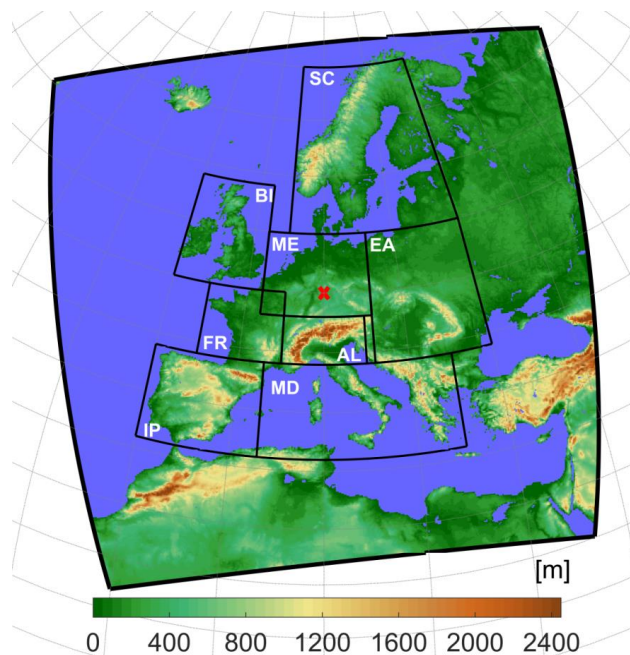
165



166 Table 1 Overview of the 19 EURO-CORDEX GCM-RCM combinations used. The rows show the GCMs while the columns
 167 show the RCMs. The full names of the RCMs are SMHI-RCA4, CLMcom-CCLM4-8-17, KNMI-RACMO22E, DMI-HIRHAM5,
 168 MPI-CSC-REMO2009 and CLMcom-ETH-COSMO-crCLIM-v1-1. Each GCM-RCM combination used is represented by a
 169 number (1, 3 or 12) indicating which realization of the GCM is used for the particular simulation.
 170

GCM \ RCM	RCA	CCLM	RACMO	HIRHAM	REMO	COSMO
ICHEC-EC-EARTH	r12		r1	r3		
MOHC-HadGEM2-ES	r1		r1	r1		
CNRM-CERFACS-CNRM-CM5	r1			r1		
MPI-M-MPI-ESM-LR	r1	r2		r1	r1	r1
IPSL-IPSL-CM5A-MR	r1					
NCC-NorESM1-M	r1			r1		r1
CCCma-CanESM2		r1				
MIROC-MIROC5		r1				

171
 172
 173



174 Figure 1 Map showing the EURO-CORDEX region (outer frame) with elevation in colours. PRUDENCE sub-regions (Christensen and
 175 Christensen 2007) used in the analysis are also shown: BI = British Isles, IP = Iberian Peninsula, FR = France, ME = Mid-Europe, SC =
 176 Scandinavia, AL = Alps, MD = Mediterranean, EA = Eastern Europe. Red cross marks point used in Figure 4.
 177
 178
 179



180 3 Methods

181 3.1 Duration

182 Extreme precipitation statistics is often described as function of the time scale involved as intensity-
183 duration-frequency or depth-duration-frequency curves (e.g. Overeem et al. 2008). We consider two time
184 scales or *durations*. One is a duration of 1 h, which is simply the time series of hourly precipitation sums
185 available in each RCM grid point. The other is a duration of 24 h, where a 24 h sum is applied in a sliding
186 window with a one hour time stepping. We will sometimes refer to these as hourly and daily duration,
187 respectively. Our daily duration corresponds to the traditional climatological practice of reporting daily
188 sums but allows heavy precipitation events to occur over two consecutive days. We also emphasize that
189 the duration, as defined here, is not the actual length of precipitation events in the model data, but is
190 merely a concept to define time scales.

191 3.2 Extreme value analysis

192 Extreme value analysis (EVA) is about estimating high quantiles of a statistical distribution from
193 observations. The theory relies on fundamental convergence properties of time series of extreme events;
194 for details we refer to Coles et al. (2001).

195
196 There are two main methodologies in EVA to obtain estimates of the high percentiles and the
197 corresponding return levels. In the *classical*, or *block maxima*, method, a generalised extreme value
198 distribution is fitted to the series of maxima over a time block, usually a year. Alternatively, in the *peak-*
199 *over-threshold* (POT) or *partial-duration-series* method, which is used here, all peaks with maximum above
200 a (high) threshold, x_0 , are considered. The peaks are assumed to occur independently at an average rate
201 per year of λ_0 . To ensure independence between peaks, a minimum time separation between peaks is
202 specified. Theory tells us, that when the threshold goes to infinity, the distribution of the exceedances
203 above the threshold, $x - x_0$, converges to a generalised Pareto distribution, whose cumulative distribution
204 function is

$$\mathcal{G}(x - x_0) = 1 - \left(1 + \xi \frac{x - x_0}{\sigma}\right)^{-\frac{1}{\xi}}, x > x_0$$

205 The parameter σ is the scale and is a measure of the width of the distribution. The parameter ξ is the shape
206 and describes the character of the upper tail of the GPD-distribution; $\xi > 0$ implies a heavy tail which
207 usually is the case for extreme precipitation events, while $\xi < 0$ implies a thin tail. Note that, quite
208 confusingly, an alternative sign convention of ξ occurs in the literature (e.g. Hosking and Wallis 1987).

209
210 If we now consider an arbitrary level x with $x > x_0$, the average number of exceedances per year of x will
211 be

$$\lambda_x = \lambda_0 [1 - \mathcal{G}(x - x_0)]. \quad (1)$$

212
213
214
215 The T -year return level, x_T , is defined as the precipitation intensity which is exceeded on average once
216 every T years

$$\lambda_{x_T} T = 1$$

217 and by combining with (1) we get an expression for the return level x_T



218

219

220 from which

221

222

223

224 Data points to be included in the POT analysis can be selected in two different ways. Either the threshold x_0
225 is specified and λ_0 is then a parameter to be determined or, alternatively, λ_0 is specified and x_0 determined
226 as a parameter. We choose the latter approach, since it is most convenient when working with data from
227 many different model simulations.

228

229 Choosing λ_0 is a point to consider: a too high value would include too few data points in the estimation and
230 a too low value implies the risk that the exceedances $x_T - x_0$ cannot be considered as GPD-distributed. We
231 choose $\lambda_0 = 3$ in accordance with Berg et al. (2019), which gives 75 data points for estimation for the 25
232 years period. Hosking and Wallis (1987) investigated the estimation of parameters of the GPD-distribution
233 and based on this warns against using the often applied maximum likelihood estimation for a sample size
234 below 500. Instead, he recommends probability-weighted moments and we have followed this advice here.

235

236 We required a minimum of 3 and 24 h separation between peaks for 1 and 24 h duration, respectively. This
237 is in accordance with Berg et al. (2019) and furthermore, synoptic experience tells us that this will ensure
238 that neighbouring peaks are from independent weather systems. We found only a weak influence of these
239 choices on the results of our analysis.

240

241 3.3 Bias adjustments and extreme value analysis

242 The delta-change and bias correction approaches were introduced in general terms in Section 1. Now we
243 will formulate EVA-based analytical quantile-mapping based versions of the two approaches. In what
244 follows O_T is the T -year return levels estimated from (pseudo-)observations during the present-day period,
245 while C_T (control) and S_T (scenario) denote the corresponding return levels, estimated from present-day
246 and end-21st-century model data, respectively. Finally, P_T (projection) denotes the end-21st-century return
247 level after bias-adjustment has been applied.

248

249 3.3.1 Climate factor on the return levels (FAC)

250 The simplest adjustment approach is to assume a climate factor on the return level (FAC)

$$P_T = \underbrace{S_T/C_T}_{\substack{\text{Delta-change} \\ \text{climate factor}}} \cdot O_T = \underbrace{O_T/C_T}_{\substack{\text{Bias correction} \\ \text{climate factor}}} \cdot S_T$$

251

252 We note that the delta-change and bias correction approach are identical for the FAC method.



253 3.3.2 Analytical quantile matching based on EVA

254 Kallache et al. (2011) and Laflamme et al. (2016) applies a transformation methodology for extreme values,
255 based on analytical quantile-matching and applicable for both the block- and the POT-methods, which will
256 be adapted to our needs below.

257

258 In the EVA-based quantile-matching, two POT-based extreme value distributions with different parameters
259 are matched. Being more specific, we want to construct a transformation $x \rightarrow y$ defined by requiring that
260 exceedance rates above x and y , respectively, are equal for any x :

$$261 \lambda_x = \lambda_y.$$

262 This implies, according to (1), that

263

$$264 \lambda_{0x}[1 - \mathcal{G}_x(x - x_0)] = \lambda_{0y}[1 - \mathcal{G}_y(y - y_0)],$$

265 where \mathcal{G}_x is the GPD distribution of the exceedances $x - x_0$ and λ_{0x} the associated exceedance rate, and
266 \mathcal{G}_y and λ_{0y} are the similar entities for y .

267

268 To simplify, we let $\lambda_{0x} = \lambda_{0y}$ (see Section 3.2) and therefore get

$$269 \mathcal{G}_x(x - x_0) = \mathcal{G}_y(y - y_0),$$

270 from which we obtain the transformation

$$271 y = y_0 + \mathcal{G}_y^{-1}(\mathcal{G}_x(x - x_0)). \quad (3)$$

272

273 For the delta-change approach (DC), the modelled GPD distribution functions for present-day and end-21st-
274 century conditions are quantile-matched and the transformation obtained this way is then applied to
275 return levels determined from present-day (pseudo-)observations O_T . Thus the corresponding projected T -
276 year return level is according to Eq. (3)

$$P_T = S_0 + \mathcal{G}_S^{-1}(\mathcal{G}_C(O_T - C_0)),$$

277 where \mathcal{G}_C and \mathcal{G}_S are the GPD cumulative distribution functions for the modelled present-day (control) and
278 end-21st-century (scenario) data, respectively, and C_0 and S_0 are the corresponding threshold values.

279

280 For the bias correction approach (BC), the present-day (control) and (pseudo-)observed GPD cumulative
281 distribution functions are quantile-matched to obtain the model bias, which then is applied, according to
282 eq. (3), to modelled end-21st-century (scenario) return levels.

283

$$284 P_T = O_0 + \mathcal{G}_O^{-1}(\mathcal{G}_C(S_T - C_0)),$$

285 where \mathcal{G}_O is the GPD cumulative distribution function for the observations and O_0 the corresponding
286 threshold.

287 3.3.3 Reference adjustment methods

288 The performance of the bias adjustment methods described above will be compared with the performance
289 of two reference adjustment methods, which are defined below. This is a similar to what is practice when
290 verifying predictions, where the performance of the prediction should be superior to the performance of
291 reference predictions, such as persistence or climatology.

292



293 We choose two reference methods. One reference is to simply use, for a given model, the return level
 294 calculated from (pseudo-)observations as the projected return level (OBS),

$$P_T = O_T$$

295

296 Another reference is to use the scenario model output without any bias adjustment (SCE):

297

$$P_T = S_T.$$

298

299 For an overview of methods, see Table 2

300

301 Table 2 Overview of methods used in the inter-comparison

OBS	(Pseudo-)observations (Reference)
SCE	Unadjusted RCM scenario (Reference)
FAC	Climate factors on return levels
DC	Quantile-matched delta-change based on EVA
BC	Quantile-matched bias correction based on EVA

302

303

304 4 Results

305

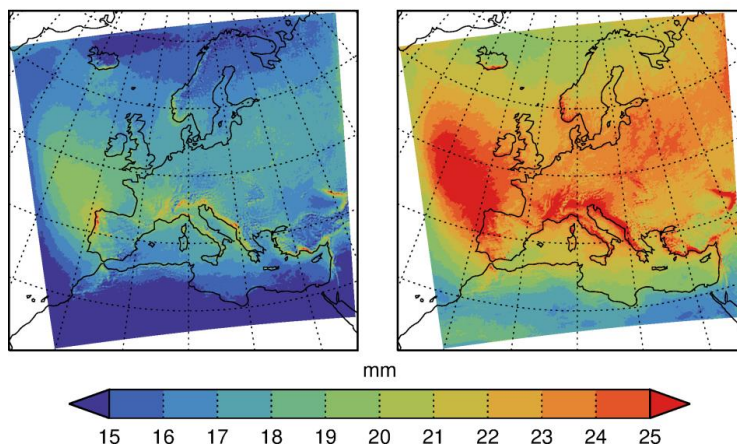
306 4.1 Modelled return levels for present-day and end-21st-century conditions

307

Return level, Duration: 1 h, Return period: 10 y

Present-day

End-21st-century



308

309 Figure 2 Geographical distribution of the 10 year-return level of precipitation intensity for 1 hour duration for present-day (left)
 310 and end-21st-century (right). In each grid point, values are the median return level over all 19 model simulations.

311

312 Figure 2 displays the geographical distribution of the 10-year return level for precipitation intensity of 1 h
 313 duration, calculated as the median return level over all 19 model simulations. There is a general increase

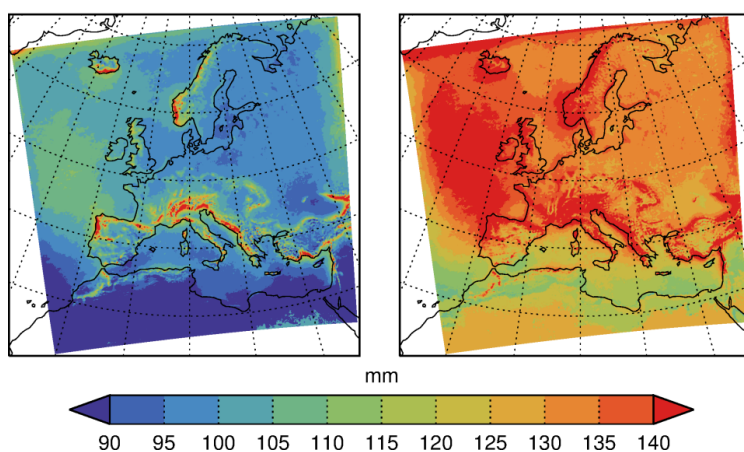


314 from present-day to end-21st-century climatic conditions. The smallest return levels are mainly found in the
 315 arid North African region and to some extent in the Norwegian Sea, while the largest return levels are
 316 found in southern Europe and in the Atlantic northwest of the Iberian Peninsula. Mountainous regions,
 317 such as the Alps and western Norway have higher return levels than their surroundings.
 318
 319

Return level, Duration: 24 h, Return period: 10 y

Present-day

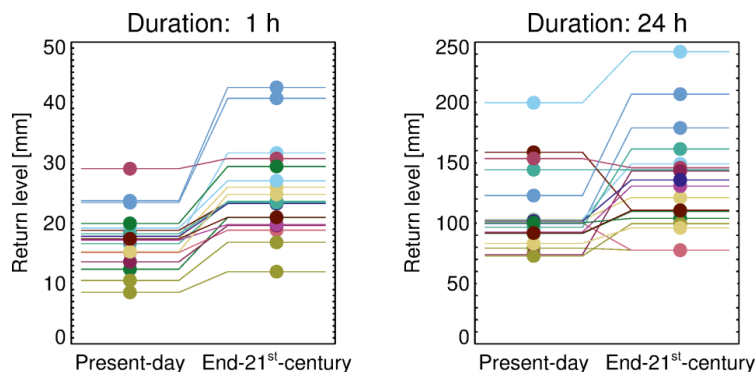
End-21st-century



320
 321 Figure 3 As Figure 2 but for 24 h duration
 322

323 We also show in Figure 3 the median 10-year return level for 24 h duration, and this shows similar
 324 qualitative characteristics: For both durations the return levels generally increase from present-day to end-
 325 21st-century conditions, although the effect is more pronounced for 1 h duration.
 326

327



328
 329 Figure 4 Modelled return levels at 50N/10E (northern Germany, marked with 'X' in Figure 1) for present and future for 10 y return
 330 period and 1 h and 24 h durations. Different colours represent the 19 different GCM-RCM simulations listed in Table 1.
 331



332 To get a more detailed impression of the data, Figure 4 shows return levels and their changes from present-
333 day to end-21st-century for a grid point in Northern Germany for all 19 model simulations. For 1 h duration
334 (left panel) return values increase from present-day to end-21st-century in all cases. For 24 h duration (right
335 panel) typically the return levels increase from present-day to end-21st-century but with some exceptions.
336 For both durations, we also note the large spread in return levels within the ensemble. The spread is much
337 higher than the change between present and future for most models; in other words: a poor signal to noise
338 ratio.

339 4.2 Inter-model cross-validation

340 4.2.1 Validation metrics

341 Results of the inter-model cross-validation are presented in this section. The basic verification metric will be
342 the relative error of future return levels for a given duration and return period T , defined as

$$343 RE = |P_T - V_T|/V_T$$

344
345 i.e. the absolute difference between the projected return level P_T obtained from applying bias adjustment
346 and the verification return level V_T estimated from end-21st-century pseudo-reality, divided by the
347 verification return level. This metric is calculated for every grid point and for every model/pseudo-reality
348 combination. Since we have $N = 19$ model simulations in the ensemble, we can make $N \times (N - 1) = 342$
349 evaluations of each bias adjustment method and make statistics of the relative error. This quantifies the
350 average performance of the different bias adjustment methods.
351

352

353 In the following, we will present results using two different types of display. First, we will use spatial maps
354 of the median relative error, calculated from all model/pseudo-reality combinations. Second, we will, for
355 each adjustment method and for each model/pseudo-reality combination, calculate the median relative
356 error over each of the eight PRUDENCE sub-regions defined in Christensen and Christensen (2007) and
357 shown on Figure 1. For each region we will illustrate the distribution of the relative error across all
358 model/pseudo-reality combinations by showing the median and the 0.05/0.95-percentiles of this
359 distribution.
360

361 4.2.2 Results for 1 h duration

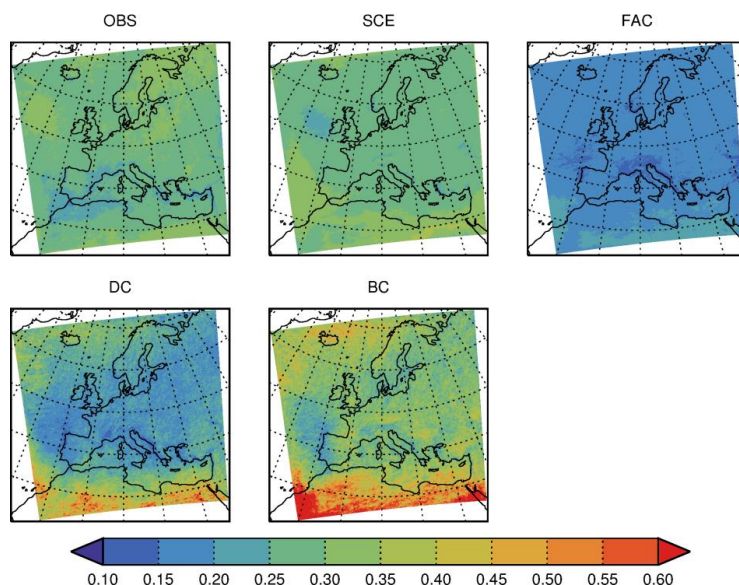
362

363 Figure 5 shows the median, across all model/pseudo-reality combinations, of RE for all five methods for 1 h
364 duration and 10 y return period.

365



Relative error, Duration: 1 h, Return period: 10 y



366

367

368

369

370

371

Figure 5 Geographical distribution of the relative error of end-21st-century 10 year return level for 1 h duration precipitation intensity from the inter-model cross-validation. Colours show the median of the relative error calculated over all model/pseudo-reality combinations. Panels are for the different bias correction methods.

372

First we look at the reference methods. The OBS method has relative errors in the approximate interval 0.2-0.4. Lowest values are found in the Mediterranean, western France and the Atlantic west of the Mediterranean; highest values in the Atlantic west of Ireland and in Scandinavia. The SCE method has errors in the interval 0.25-0.45, lowest values in the Atlantic west of Ireland; largest values over parts of the Atlantic and northern Africa. Of the two reference methods, the OBS method outperforms SCE in the south, while the opposite is true in the north.

378

379

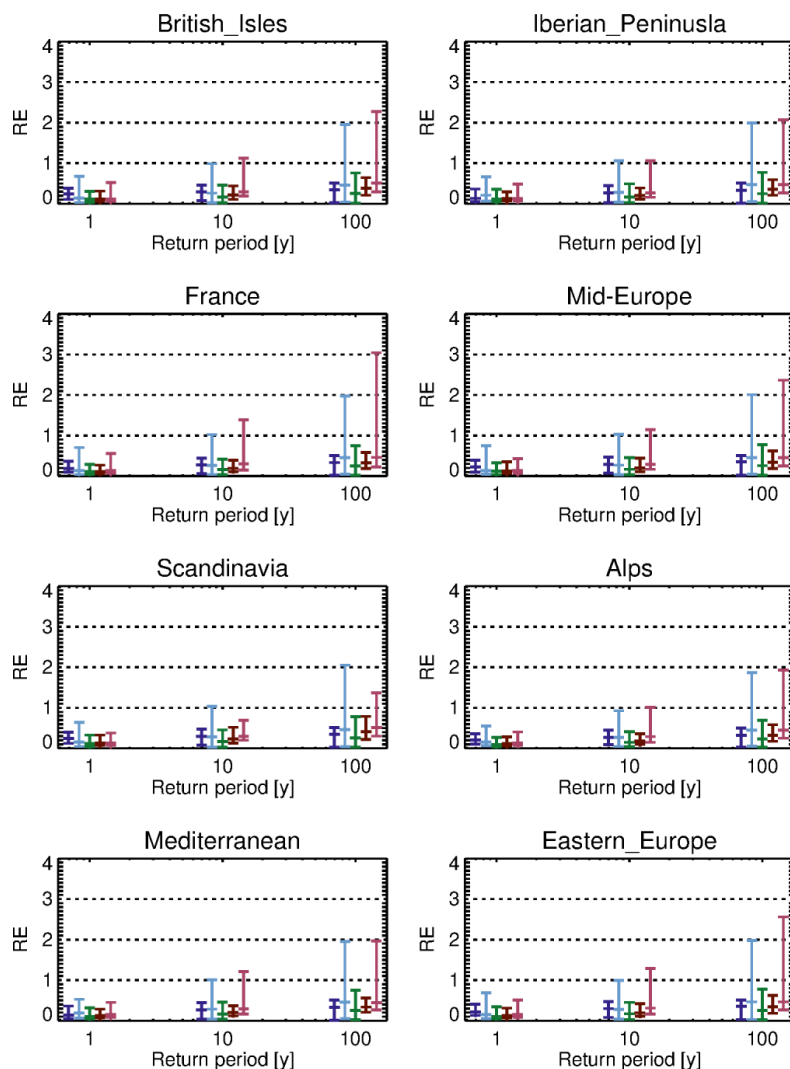
The relative error of FAC is below 0.2 in most places. It is everywhere smaller than the relative error of the reference methods OBS and SCE. The DC method has a relative error comparable to (e.g. Western France, Western Iberia and Eastern Atlantic) or larger than (in particular in Northern Africa) that of FAC. That said, the concept of relative error should be used with care in an arid region, such as Northern Africa. But from this result, it is not justified to use the more complicated DC, in favour of the simpler FAC. Finally, the relative error of BC is everywhere above both DC and FAC, indicating the poorest performance of all methods considered.

385

386



Relative error, Duration: 1 h



OBS SCE FAC DC BC

387
 388
 389
 390
 391

Figure 6 Statistical distribution (median and .05/.95-fractiles) of the relative error of the inter-model cross-validation for 1 hour duration for 1 y, 10 y and 100 y return periods. Panels represent PRUDENCE sub-regions shown in Figure 1. Each colour represents an adjustment method (see Table 2).

392
 393
 394
 395
 396

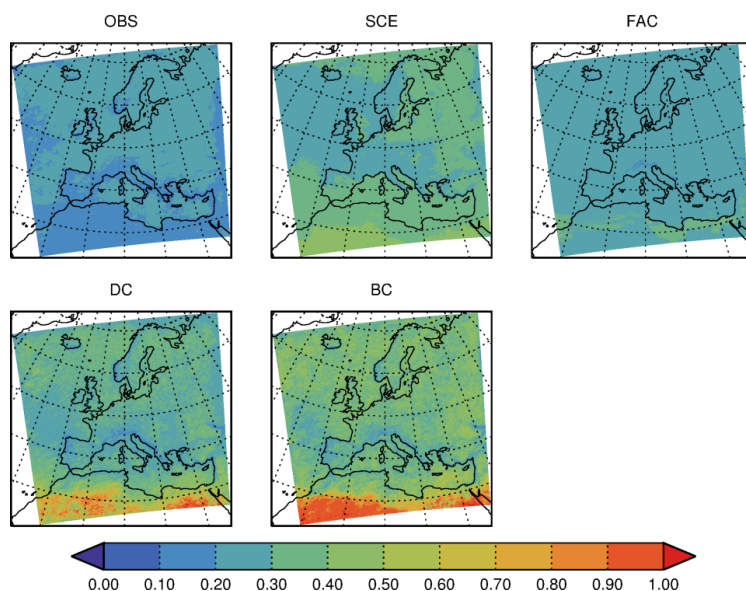
The statistical distribution of the relative error is shown in Figure 6 for the eight PRUDENCE sub-regions (see Figure 1). We first note that the distribution of relative error is shifted towards higher values for larger return periods, as expected. Next, we note that the two reference methods, OBS and SCE, behave differently. SCE generally has a little larger median relative error, but the .95-fractile is much larger for SCE than for OBS, in particular for large return periods. Thus, OBS overall performs better than SCE, meaning



397 that using present-day pseudo-observations to estimate projected end-21st-century return levels yields
398 better relative error than using raw modelled scenario data.
399
400 The FAC method generally has the best overall performance, both in terms of median and .95-fractile of the
401 relative error. Of the two quantile-matching methods, the DC method has a slightly poorer performance
402 than FAC, both in terms of the median and the .95-fractile of the relative error. Finally, BC has poorer
403 performance than DC, when comparing the median of the relative error and in particular for the .95-
404 fractile.
405
406 In summary, for 1 h duration, the method with the best performance is using a climate factor on the return
407 levels (FAC). This method outperforms both reference methods and the more sophisticated methods based
408 on quantile-matching, DC and BC, the latter having the poorest overall performance of them all.
409

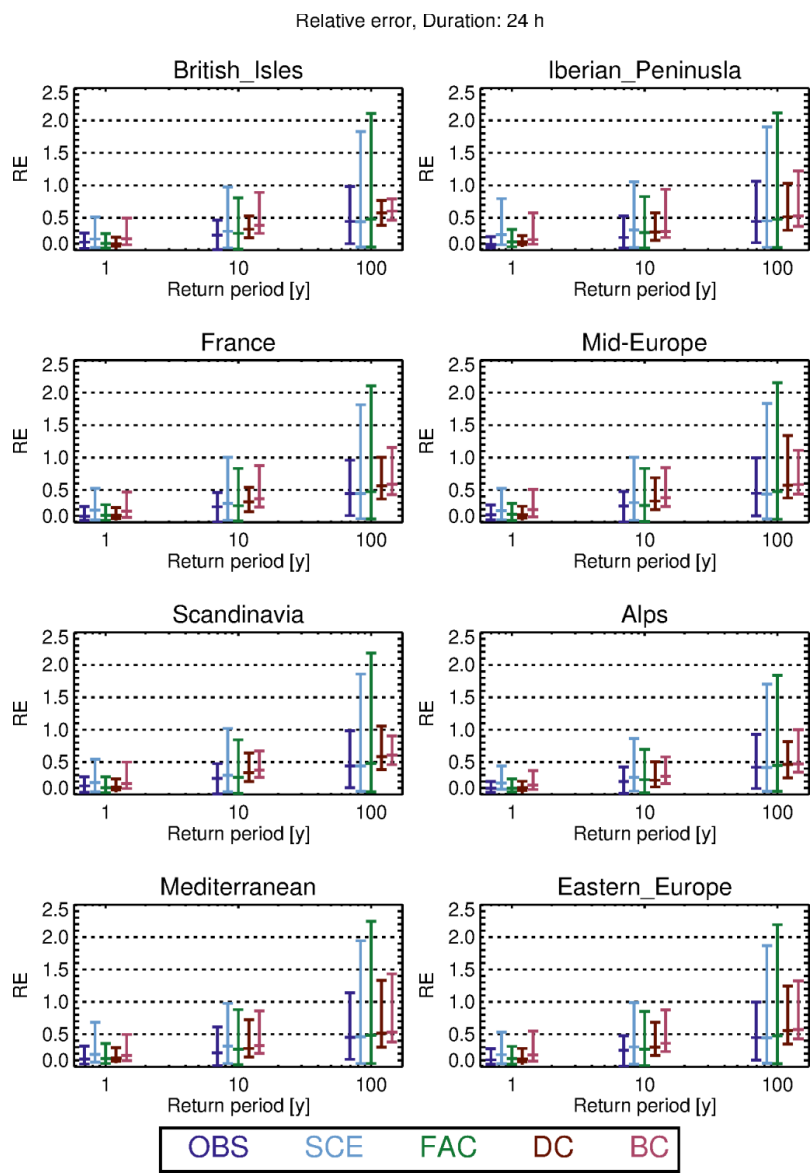
410 4.2.3 Results for 24 h duration 411

Relative error, Duration: 24 h, Return period: 10 y



412
413 Figure 7 As Figure 5 but for 24 h duration.
414
415

416 For 24 h duration (see Figure 7), OBS has the lowest median relative error (lower than 0.3) in most regions
417 of all the adjustment methods, while SCE has higher relative error in the interval 0.3-0.6 approximately,
418 with the highest values in North Africa. FAC has relative errors between OBS and SCE. Of the quantile-
419 matching methods, DC has relative errors in the interval 0.2-0.8 approximately, larger than FAC in most
420 places, and finally BC has, as for 1 h duration, the largest median relative errors of all the methods.
421



422
 423
 424

Figure 8 As Figure 6 but for 24 h duration

425 As for the 1 h duration, we also compare the entire statistical distribution of the relative error of the
 426 different adjustment methods for all three return periods (Figure 8), and again, both median and .95-
 427 fraction of the relative error increases for larger return periods, as expected. Further, OBS seems,
 428 surprisingly, to have a small median relative error and the smallest .95-fractile of all methods considered
 429 for all sub-regions. SCE has a median not too different from that of OBS, but the .95-fractile is much larger.



430 Similar characteristics hold for FAC. The quantile-matching methods DC and BC have slightly larger median
 431 values, but the .95-fractile is smaller than for FAC. All these characteristics hold for all sub-regions.

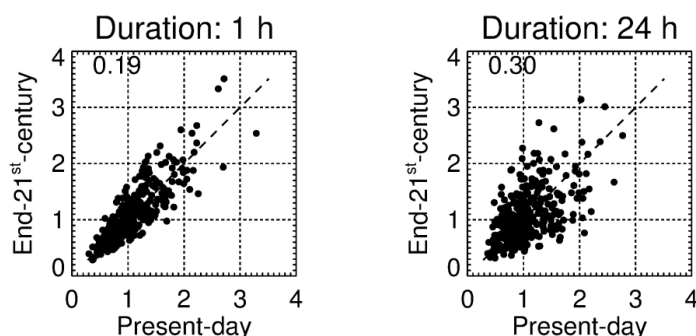
432 4.3 Further analysis on conditions for skill

433

434 To get further insight into the difference in performance between hourly and daily precipitation, we
 435 consider the relationship between the bias factor for present-day $B_P = \frac{C}{O}$ and end-21st-century $B_F = \frac{S}{V}$ for
 436 all model/pseudo-reality combinations (see Figure 9).

437

Bias factor of return level, Region: Mid-Europe Return period: 10 y



438 Figure 9 Relationship between present-day and end-21st-century bias factors of 10-year return levels for Mid-Europe sub-region for
 439 all pseudo-observation/model combinations. Left panel: 1 h duration and right panel: 24 h duration. Numbers in upper left corners
 440 are the R measure of relative spread. See text for details.
 441
 442

443 In this figure, the relationship between present-day and end-21st-century bias factors appears more
 444 pronounced for 1 h duration than for 24 h duration. That said, it must be borne in mind that if the point
 445 (x, y) is in the plot, so is the point $(1/y, 1/x)$, and this implies an inherent tendency to a fan-like spread of
 446 points from $(0,0)$, as seen on both plots.

447

448 Therefore, to quantify the relationship we use the measure of the relative spread introduced by Maurer et
 449 al. (2013):

450
$$R = \left\langle \frac{|B_F - B_P|}{(B_F + B_P)/2} \right\rangle,$$

451 where $\langle \cdot \rangle$ means averaging over model/pseudo-reality combinations. These R -values, given in the upper
 452 left corner of each panel, also support the partial relationships described above, and a stronger one for
 453 hourly duration.

454

455 These relations are important since they could explain the generally good performance of the FAC
 456 adjustment methods seen in the previous section. Suppose that $B_P = B_F$, then

457
$$P_T = \frac{S_T}{C_T} O_T = S_T \frac{O_T}{C_T} = S_T B_P = S_T B_F = S_T \frac{V_T}{S_T} = V_T$$

458

459 and the FAC method will therefore adjust perfectly.



460

461 We also note that daily data, due to the summation, would have less erratic behaviour than hourly and
462 therefore we would expect any relationship to be less masked by noise for daily data than for hourly data
463 from purely statistical grounds. Therefore, any explanation to why it is opposite should probably be found
464 in physics or details of modelling. We will discuss this further in Section 5.3.

465 **5 Discussion**

466

467 **5.1 Relation with other studies**

468

469 The study by Rätty et al. (2014) touches upon related issues to ours. However, our study includes smaller
470 temporal scales (hourly and daily) than does their study and higher return periods (up to 100 years vs. the
471 .999-fractile of daily precipitation corresponding to a return period of around 3 years). Nevertheless, the
472 two studies agree in their main conclusion; namely that applying a bias adjustment seems to offer an
473 additional level of realism to the processed data series, including in the climate projections, as compared to
474 using unadjusted model results. The two studies also both support the somewhat surprising conclusion
475 that, using present-day observations as the scenario gives a skill comparable to that of the bias adjustment
476 methods.

477

478 Another relevant study to discuss here is Laflamme et al. (2016) who apply the BC method similar to ours to
479 daily data from different model runs and concludes that “downscaled results are highly dependent on RCM
480 and GCM model choice”. Finally, Kallache et al. (2011) obtained good result with the BC in a
481 training/verification split of historical data.

482

483 **5.2 Convection in RCMs**

484 The grid spacing of present state-of-the-art RCMs available in large ensembles, such as CORDEX, is around
485 10 km, and at this resolution it is necessary to describe convection through parameterizations. This is
486 obviously an important deficit for our purpose, since this could represent a systematic bias in all our
487 simulations and therefore violate our underlying assumptions that the individual model simulations and the
488 real-world observations behave approximately similar in a physical sense.

489

490 With the advent of convective-permitting models, a more realistic modelling of convective precipitation
491 events is within reach and a change in the characteristics of such events is seen (Kendon et al. 2017;
492 Lenderink et al. 2019; Prein et al. 2015). This next generation of convection-permitting RCMs with a grid
493 spacing of a few km allows a much better representation of the diurnal cycle and convective systems as a
494 whole (Prein et al. 2015). With that in mind, we foresee redoing the analysis when a suitable ensemble of
495 convective-permitting RCM simulations becomes available.

496



497 **5.3 Stationarity of bias**

498 The success of applying bias adjustment to climate model simulations is linked to the biases being
499 stationary, i.e. present and future biases being more or less identical. In Section 4.3 we showed (in Figure 9)
500 that this was the case for 1 h duration and less so for 24 h duration in our pseudo-reality setting. Such a
501 relationship is an example of an emergent constraint (Collins et al. 2012). This is a model-based concept,
502 originally introduced to explain that models which have a too warm (cold) present-day climate tend to have
503 a relatively warmer (colder) future climate. The reason for this is that it is the same underlying physics
504 which generates the present-day and future temperatures (Christensen and Boberg 2012). It has also been
505 shown that on monthly time scales, the precipitation bias in Scandinavia depends on the precipitation
506 (Christensen et al. 2008).

507
508 We suggest that our observed emergent constraints could be explained in a similar manner; namely as a
509 result of the Clausius-Clapeyron relation linking atmospheric temperature changes to changes in its
510 humidity content and thereby precipitation changes. The change prescribed by the Clausius-Clapeyron
511 equation is usually termed the thermodynamic contribution. In addition to this, there is a dynamic
512 contribution and this may explain the differences between the hourly and daily relation seen in Figure 9.
513 The rationale is that hourly extremes are entirely due to convective precipitation events with almost no
514 dynamic contribution (Lenderink et al. 2019), while daily extremes are a mixture of convective events and
515 large-scale strong precipitation, of which the latter has a more significant dynamic contribution (Pfahl et al.
516 2017), causing the less marked emergent constraint for the daily time scale. This interpretation is also
517 supported in Figure 4, in which daily precipitation sees some ‘crossovers’ (future return level smaller than
518 present), whereas hourly precipitation does not have any crossovers.
519

520 **5.4 The spatial scale**

521 In the definition of model bias it is tacitly assumed that the observational dataset has the same spatial
522 resolution as the model data. In practice, however, it is rarely possible to separate the bias from a spatial
523 scale mismatch. For instance, if we compare modelled precipitation, which represents averages over a grid
524 box, with rain gauge data, which represent a point, there can be a quite substantial mismatch for extreme
525 events (Eggert et al. 2015; Haylock et al. 2008). Therefore, if the bias is adjusted towards such point values,
526 it may lead to further complications (Maraun 2013).

527
528 Sometimes though, it is desirable to include the scale mismatch in the bias adjustment. Many impact
529 models, e.g. hydrological models, are tuned to perform well with local observational data as input. This
530 presents an additional challenge if this impact model is to be driven by climate model data for climate
531 change studies, since the climate model will have biases in its climate characteristics (mean, variability, etc.)
532 compared to those of the observed data. Applying the bias adjustment step, the hydrological model can
533 rely on its calibration to observed conditions (Refsgaard et al. 2014; Haerter et al. 2015).
534

535 **6 Conclusions**

536



537 Based on hourly precipitation data from a 19-member ensemble of climate simulations we have
538 investigated the benefit of bias adjusting extreme precipitation return levels on hourly and daily time scales
539 and evaluated the different methods. This is done in a pseudo-reality setting, where one model simulation
540 in turn from the ensemble plays the role of observations extending into the future. The return levels
541 obtained from each of the remaining model simulations are then bias adjusted in the present-day period,
542 using different adjustment methods. Then the same adjustment methods are applied to end-21st-century
543 model data to obtain projected return levels, which are then compared with the corresponding pseudo-
544 realistic future return levels.

545
546 The main result of this inter-comparison is that applying bias adjustment methods improves projected
547 extreme precipitation return levels, compared to using the un-adjusted model runs. Can an overall superior
548 adjustment methodology be appointed? For hourly duration, the method to recommend (having the
549 smallest relative error) is the simple climate factor approach FAC, which is better in terms of the relative
550 error than the more complicated analytical quantile mapping methods based on EVA, DC and, in particular,
551 BC. For daily duration, the OBS method performs surprisingly well, having the smallest .95-fractile relative
552 error. Furthermore, the quantile methods perform better than FAC, with DC having the smallest relative
553 error. These conclusions hold regardless of the sub-region considered.

554
555 Finally, we registered emergent constraints between present-day and end-21st-century biases. This was
556 more pronounced for hourly than for daily time scale. This could be caused by hourly precipitation being
557 more directly linked to the Clausius-Clapeyron response, but this requires more clarification in future work.

558
559
560 *Data availability.* The hourly EURO-CORDEX precipitation data are not part of the standard suite of CORDEX
561 and are therefore not produced nor shared by all modelling groups. The data used in this study may be
562 obtained upon request from each modelling group. The IDL code used in the analysis can be obtained from
563 TS.

564
565
566 *Author contribution.* TS and PT designed the analysis with contribution from other co-authors and
567 programmed the analysis software. PB, FB, OBC and PT prepared the data. TS prepared the manuscript with
568 contributions from PT, PB, FB, OBC, BC, JHC, CS, and MSM.

569
570 *Competing interests.* The authors declare that they have no conflict of interest.

571
572 *Acknowledgements.* The work was supported by the European Commission through the Horizon 2020
573 Programme for Research and Innovation under the EUCP project (Grant Agreement 776613). Part of the
574 funding was provided by the Danish State through the Danish Climate Atlas. Some of the simulations were
575 performed in the COPERNICUS C3S project C3S_34b (PRINCIPLES). We acknowledge the World Climate
576 Research Programme's Working Group on Regional Climate, and the Working Group on Coupled Modelling,
577 former coordinating body of CORDEX and responsible panel for CMIP5. We also thank the climate
578 modelling groups (listed in Table 1 of this paper) for producing and making their model output available.
579 We also acknowledge the Earth System Grid Federation infrastructure an international effort led by the U.S.
580 Department of Energy's Program for Climate Model Diagnosis and Intercomparison, the European Network
581 for Earth System Modelling and other partners in the Global Organisation for Earth System Science Portals



582 (GO-ESSP). It is appreciated that Geert Lenderink, KNMI, Claas Teichmann, GERICS and Heimo Truhetz,
583 University of Graz made model data of hourly precipitation available for analysis.

584

585

586 References

587

588 Berg, P., H. Feldmann, and H.-J. Panitz, 2012: Bias correction of high resolution regional climate model data.
589 *J. Hydrol.*, **448–449**, 80–92, <https://doi.org/10.1016/j.jhydrol.2012.04.026>.

590 Berg, P., O. B. Christensen, K. Klehmet, G. Lenderink, J. Olsson, C. Teichmann, and W. Yang, 2019:
591 Summertime precipitation extremes in a EURO-CORDEX 0.11° ensemble at an hourly resolution.
592 *Nat. Hazards Earth Syst. Sci.*, **19**, 957–971, <https://doi.org/10.5194/nhess-19-957-2019>.

593 Boberg, F., and J. H. Christensen, 2012: Overestimation of Mediterranean summer temperature projections
594 due to model deficiencies. *Nat. Clim Change*, **2**, 433–436.

595 Buser, C., H. Künsch, and C. Schär, 2010: Bayesian multi-model projections of climate: generalization and
596 application to ENSEMBLES results. *Clim. Res.*, **44**, 227–241, <https://doi.org/10.3354/cr00895>.

597 Christensen, J. H., and O. B. Christensen, 2007: A summary of the PRUDENCE model projections of changes
598 in European climate by the end of this century. *Clim. Change*, **81**, 7–30,
599 <https://doi.org/10.1007/s10584-006-9210-7>.

600 Christensen, J. H., and F. Boberg, 2012: Temperature dependent climate projection deficiencies in CMIP5
601 models. *Geophys. Res. Lett.*, **39**, 24705, <https://doi.org/10.1029/2012GL053650>.

602 —, —, O. B. Christensen, and P. Lucas-Picher, 2008: On the need for bias correction of regional climate
603 change projections of temperature and precipitation. *Geophys. Res. Lett.*, **35**,
604 <https://doi.org/10.1029/2008GL035694>.

605 Coles, S., J. Bawa, L. Trenner, and P. Dorazio, 2001: *An introduction to statistical modeling of extreme*
606 *values*. Springer,.

607 Collins, M., R. E. Chandler, P. M. Cox, J. M. Huthnance, J. Rougier, and D. B. Stephenson, 2012: Quantifying
608 future climate change. *Nat. Clim. Change*, **2**, 403–409, <https://doi.org/10.1038/nclimate1414>.

609 Eggert, B., P. Berg, J. O. Haerter, D. Jacob, and C. Moseley, 2015: Temporal and spatial scaling impacts on
610 extreme precipitation. *Atmospheric Chem. Phys.*, **15**, 5957–5971, <https://doi.org/10.5194/acp-15-5957-2015>.

612 Eyring, V., S. Bony, G. A. Meehl, C. A. Senior, B. Stevens, R. J. Stouffer, and K. E. Taylor, 2016: Overview of
613 the Coupled Model Intercomparison Project Phase 6 (CMIP6) experimental design and
614 organization. *Geosci. Model Dev.*, **9**, 1937–1958, <https://doi.org/10.5194/gmd-9-1937-2016>.

615 Haerter, J. O., S. Hagemann, C. Moseley, and C. Piani, 2011: Climate model bias correction and the role of
616 timescales. *Hydrol. Earth Syst. Sci.*, **15**, 1065–1079, <https://doi.org/10.5194/hess-15-1065-2011>.

617 Haerter, J. O., B. Eggert, C. Moseley, C. Piani, and P. Berg, 2015: Statistical precipitation bias correction of
618 gridded model data using point measurements. *Geophys. Res. Lett.*, **42**, 1919–1929,
619 <https://doi.org/10.1002/2015GL063188>.



- 620 Hanel, M., and T. A. Buishand, 2010: On the value of hourly precipitation extremes in regional climate
621 model simulations. *J. Hydrol.*, **393**, 265–273, <https://doi.org/10.1016/j.jhydrol.2010.08.024>.
- 622 Haylock, M. R., N. Hofstra, A. M. G. Klein Tank, E. J. Klok, P. D. Jones, and M. New, 2008: A European daily
623 high-resolution gridded data set of surface temperature and precipitation for 1950–2006. *J.*
624 *Geophys. Res.*, **113**, <https://doi.org/10.1029/2008JD010201>.
- 625 Hosking, J. R. M., and J. R. Wallis, 1987: Parameter and Quantile Estimation for the Generalized Pareto
626 Distribution. *Technometrics*, **29**, 339, <https://doi.org/10.2307/1269343>.
- 627 Jacob, D., and Coauthors, 2014: EURO-CORDEX: new high-resolution climate change projections for
628 European impact research. *Reg. Environ. Change*, **14**, 563–578, [https://doi.org/10.1007/s10113-](https://doi.org/10.1007/s10113-013-0499-2)
629 013-0499-2.
- 630 Kallache, M., M. Vrac, P. Naveau, and P.-A. Michelangeli, 2011: Nonstationary probabilistic downscaling of
631 extreme precipitation. *J. Geophys. Res.*, **116**, <https://doi.org/10.1029/2010JD014892>.
- 632 Kendon, E. J., N. M. Roberts, H. J. Fowler, M. J. Roberts, S. C. Chan, and C. A. Senior, 2014: Heavier summer
633 downpours with climate change revealed by weather forecast resolution model. *Nat. Clim. Change*,
634 **4**, 570–576, <https://doi.org/10.1038/nclimate2258>.
- 635 —, and Coauthors, 2017: Do Convection-Permitting Regional Climate Models Improve Projections of
636 Future Precipitation Change? *Bull. Am. Meteorol. Soc.*, **98**, 79–93, [https://doi.org/10.1175/BAMS-D-](https://doi.org/10.1175/BAMS-D-15-0004.1)
637 15-0004.1.
- 638 Laflamme, E. M., E. Linder, and Y. Pan, 2016: Statistical downscaling of regional climate model output to
639 achieve projections of precipitation extremes. *Weather Clim. Extrem.*, **12**, 15–23,
640 <https://doi.org/10.1016/j.wace.2015.12.001>.
- 641 Lenderink, G., D. Belušić, H. J. Fowler, E. Kjellström, P. Lind, E. van Meijgaard, B. van Ulft, and H. de Vries,
642 2019: Systematic increases in the thermodynamic response of hourly precipitation extremes in an
643 idealized warming experiment with a convection-permitting climate model. *Environ. Res. Lett.*, **14**,
644 074012, <https://doi.org/10.1088/1748-9326/ab214a>.
- 645 Maraun, D., 2012: Nonstationarities of regional climate model biases in European seasonal mean
646 temperature and precipitation sums. *Geophys. Res. Lett.*, **39**, n/a-n/a,
647 <https://doi.org/10.1029/2012GL051210>.
- 648 Maraun, D., 2013: Bias Correction, Quantile Mapping, and Downscaling: Revisiting the Inflation Issue. *J.*
649 *Clim.*, **26**, 2137–2143, <https://doi.org/10.1175/JCLI-D-12-00821.1>.
- 650 —, 2016: Bias Correcting Climate Change Simulations - a Critical Review. *Curr. Clim. Change Rep.*, **2**, 211–
651 220, <https://doi.org/10.1007/s40641-016-0050-x>.
- 652 —, and Coauthors, 2017: Towards process-informed bias correction of climate change simulations. *Nat.*
653 *Clim. Change*, **7**, 764–773, <https://doi.org/10.1038/nclimate3418>.
- 654 Maurer, E. P., T. Das, and D. R. Cayan, 2013: Errors in climate model daily precipitation and temperature
655 output: time invariance and implications for bias correction. *Hydrol. Earth Syst. Sci.*, **17**, 2147–2159,
656 <https://doi.org/10.5194/hess-17-2147-2013>.



- 657 Olsson, J., P. Berg, and A. Kawamura, 2015: Impact of RCM Spatial Resolution on the Reproduction of Local,
658 Subdaily Precipitation. *J. Hydrometeorol.*, **16**, 534–547, <https://doi.org/10.1175/JHM-D-14-0007.1>.
- 659 Overeem, A., A. Buishand, and I. Holleman, 2008: Rainfall depth-duration-frequency curves and their
660 uncertainties. *J. Hydrol.*, **348**, 124–134, <https://doi.org/10.1016/j.jhydrol.2007.09.044>.
- 661 Pfahl, S., P. A. O’Gorman, and E. M. Fischer, 2017: Understanding the regional pattern of projected future
662 changes in extreme precipitation. *Nat. Clim. Change*, **7**, 423–427,
663 <https://doi.org/10.1038/nclimate3287>.
- 664 Piani, C., J. O. Haerter, and E. Coppola, 2010: Statistical bias correction for daily precipitation in regional
665 climate models over Europe. *Theor. Appl. Climatol.*, **99**, 187–192, <https://doi.org/10.1007/s00704-009-0134-9>.
666
- 667 Prein, A. F., and Coauthors, 2015: A review on regional convection-permitting climate modeling:
668 Demonstrations, prospects, and challenges. *Rev. Geophys.*, **53**, 323–361,
669 <https://doi.org/10.1002/2014RG000475>.
- 670 Räisänen, J., and O. Räty, 2013: Projections of daily mean temperature variability in the future: cross-
671 validation tests with ENSEMBLES regional climate simulations. *Clim. Dyn.*, **41**, 1553–1568,
672 <https://doi.org/10.1007/s00382-012-1515-9>.
- 673 Räty, O., J. Räisänen, and J. S. Ylhäisi, 2014: Evaluation of delta change and bias correction methods for
674 future daily precipitation: intermodel cross-validation using ENSEMBLES simulations. *Clim. Dyn.*, **42**,
675 2287–2303, <https://doi.org/10.1007/s00382-014-2130-8>.
- 676 Refsgaard, J. C., and Coauthors, 2014: A framework for testing the ability of models to project climate
677 change and its impacts. *Clim. Change*, **122**, 271–282, <https://doi.org/10.1007/s10584-013-0990-2>.
- 678 Sunyer, M., J. Luchner, C. Onof, H. Madsen, and K. Arnbjerg-Nielsen, 2017: Assessing the importance of
679 spatio-temporal RCM resolution when estimating sub-daily extreme precipitation under current
680 and future climate conditions. *Int. J. Climatol.*, **37**, 688–705.
- 681 Taylor, K. E., R. J. Stouffer, and G. A. Meehl, 2012: An Overview of CMIP5 and the Experiment Design. *Bull.*
682 *Am. Meteorol. Soc.*, **93**, 485–498, <https://doi.org/10.1175/BAMS-D-11-00094.1>.
- 683 Themeßl, M. J., A. Gobiet, and A. Leuprecht, 2011: Empirical-statistical downscaling and error correction of
684 daily precipitation from regional climate models. *Int. J. Climatol.*, **31**, 1530–1544,
685 <https://doi.org/10.1002/joc.2168>.
- 686 —, —, and G. Heinrich, 2012: Empirical-statistical downscaling and error correction of regional climate
687 models and its impact on the climate change signal. *Clim. Change*, **112**, 449–468,
688 <https://doi.org/10.1007/s10584-011-0224-4>.
- 689 Trenberth, K. E., A. Dai, R. M. Rasmussen, and D. B. Parsons, 2003: The Changing Character of Precipitation.
690 *Bull. Am. Meteorol. Soc.*, **84**, 1205–1218, <https://doi.org/10.1175/BAMS-84-9-1205>.
- 691